JOURNAL OF GEOPHYSICAL RESEARCH, VOL. 113, A08309, doi:10.1029/2007JA013012, 2008

Click Here for Full Article

The midlatitude F2 layer during solar eclipses: Observations and modeling

Huijun Le,[1,2] Libo Liu,[1] Xinan Yue,[1,2] and Weixing Wan[1]

Received 28 December 2007; revised 14 May 2008; accepted 30 May 2008; published 19 August 2008.

[1] We conducted a statistical analysis on the changes in foF2 during seven eclipse events on the basis of the data derived from 23 ionosonde stations. To model eclipse effects on the ionosphere, we constructed a solar spectrum model for solar eclipses. The background hmF2, local time, solar cycle, and dip angle effects on the ionospheric response to solar eclipses are investigated in the four controlled case studies. Both the measurements and simulations show that the eclipse effect is larger in the midday than in the morning and afternoon and that larger dip angle results in smaller eclipse effect. Furthermore, the simulated results show that the local time effect is actually due to the neutral concentration effect. Compared to at low solar activity, the eclipse effect in the F2 region is larger at high solar activity. This solar cycle effect is caused by the differences not only in the solar radiation but also in the background neutral gas concentration. In addition, an eclipse will produce a smaller change in NmF2 if the hmF2 is higher. In conclusion, the central finding of this paper is that most of the observed differences in the behavior of NmF2 during eclipses can be attributed to the differences in O^+ loss rate brought about by the background differences in the neutral molecular densities. The solar zenith angle, local time, and dip angle effects should be explained from this starting point.

Citation: Le, H., L. Liu, X. Yue, and W. Wan (2008), The midlatitude F2 layer during solar eclipses: Observations and modeling, *J. Geophys. Res.*, *113*, A08309, doi:10.1029/2007JA013012.

1. Introduction

[2] This paper studies the local time and solar zenith angle, solar cycle, dip angle, and background hmF2 effects on the ionospheric responses to a solar eclipse by running a midlatitude and low-latitude theoretical ionospheric model in four controlled case studies and comparing the results with ionosonde measurements during seven total solar eclipse events from 1970 to 2005. To model eclipse effects on the ionosphere, we constructed a solar spectrum model for solar eclipses and applied it to the theoretical ionospheric model. The central finding of this paper is that most of the observed differences in behavior of NmF2 during eclipses can be attributed to differences in O^+ loss rate brought about by the background differences in the neutral molecular densities. The solar zenith angle, local time, and dip angle effects should be explained from this starting point.

[3] During the past decades, the ionospheric responses to a solar eclipse have been studied extensively with various methods, such as the Faraday rotation measurement, ionosonde network, incoherent scatter radar (ISR), Global Positioning System (GPS), and satellite measurements [e.g., *Evans*, 1965a, 1965b; *Klobuchar and Whitney*, 1965; *Rishbeth*, 1968; *Hunter et al.*, 1974; *Oliver and Bowhill*, 1974; *Cohen*, 1984; *Salah et al.*, 1986; *Cheng et al.*, 1992; *Tsai and Liu*, 1999; *Huang et al.*, 1999; *Afraimovich et al.*, 1998, 2002; *Farges et al.*, 2001, 2003; *Tomás et al.*, 2007; *Adeniyi et al.*, 2007]. These studies have shown that there is an almost consistent behavior at low altitudes where there are larger depletions in electron concentration during solar eclipses and the change in electron concentration is almost synchronous with the phase of an eclipse.

[4] As is known, the ionospheric behavior at low altitudes (the E and F1 regions) is governed by photochemical processes, so the decrease of solar radiation during a solar eclipse leads to the decrease in electron production rate and electron concentration. For example, *Le et al.* [2008] studied the behaviors in the E and F1 region at middle latitude with data from thirteen European ionosonde stations for the 11 August 1999 total eclipse and also simulated the ionospheric behavior by using a midlatitude and low-latitude theoretical ionospheric model [*Yue et al.*, 2008]. Both the observed and simulated results show that the decrease in electron concentration is greater in the F1 region than in the E region.

[5] During different eclipse events, the F2 region behavior may be quite different accompanied with various amplitudes of decrease or even a small increase in the electron concentration. *Higgs* [1942] and *Pierce* [1948] reported that during the total solar eclipse of 1 October 1940 there was an increase in foF2 followed by a decrease. *Evans* [1965b] also found a similar feature of *foF*2 (F2-layer critical frequency) for the 20 July 1963 total eclipse at three ionosonde stations. In these two cases the obscurations were close to 100% at

[1]Beijing National Observatory of Space Environment, Institute of Geology and Geophysics, Chinese Academy of Sciences, Beijing, China.
[2]Graduate School of the Chinese Academy of Sciences, Beijing, China.

Copyright 2008 by the American Geophysical Union.
0148-0227/08/2007JA013012$09.00

Table 1. Station Coordinates, The Corresponding Maximum Obscuration at 200 km, and the Local Time of Maximum Obscuration

Date	Station	Geographic Latitude	Geographic Longitude	Local Time of Maximum Obscuration	Obscuration at 200 km (%)
7 March 1970	Wallops Island	37.9	284.5	1338	99
7 March 1970	Ottawa	45.4	284.1	1340	81
29 April 1976	Karaganda	49.8	73.1	1645	62
29 April 1976	Novokazalinsk	45.5	62.0	1558	76
29 April 1976	Alma ata	43.3	76.9	1710	76
29 April 1976	Tbilisi	41.7	44.8	1430	90
29 April 1976	Moscow	55.5	37.3	1341	51
26 February 1979	Ottawa	45.4	284.1	1213	81
26 February 1979	Boulder	40.0	254.7	0921	92
31 July 1981	Magadan	60.0	151.0	1358	74
31 July 1981	Karaganda	49.8	73.1	0720	97
31 July 1981	Novosibirsk	54.6	83.2	0813	98
31 July 1981	Sverdlovsk	56.4	58.6	0627	81
31 July 1981	Irkutsk	52.5	104.0	1001	93
31 July 1981	Tomsk	56.5	84.9	0824	94
30 May 1984	Wallops Island	37.9	284.5	1146	99
11 August 1999	Juliusruh	54.6	13.4	1133	82
11 August 1999	Rostov	47.2	39.7	1357	81
11 August 1999	Sofia	42.7	23.4	1237	96
11 August 1999	Tortosa	40.4	0.3	1018	75
11 August 1999	Rome	41.8	12.5	1132	85
11 August 1999	Chilton	51.6	358.7	1012	95
3 October 2005	San vito	40.7	17.9	1033	67

F1 region heights and their observations were made at locations with large magnetic dip angles. Evans proposed that two necessary (but possibly not sufficient) conditions for an increase in *foF*2 during a solar eclipse: first, the eclipse should be total or very nearly so (>90%), at F1 region heights; secondly, the magnetic dip should be large ($I > 60^\circ$). It should be noted that many previous studies with various measurements [e.g., *Datta et al.*, 1959; *Walker et al.*, 1991; *Cheng et al.*, 1992; *Boitman et al.*, 1999; *Huang et al.*, 1999; *Korenkov et al.*, 2003b; *Afraimovich et al.*, 2002; *Baran et al.*, 2003] show that most of the NmF2 (peak electron concentration in the F2-layer) decreases during solar eclipses, whereas the amplitude of *foF*2 decrease varies greatly from 0.2 MHz to 1.6 MHz, and the delay time varies from 9.5 min to 30 min. Such a great difference may be induced by background differences in neutral gas and geophysical conditions (such as solar activity and geomagnetic activity level), and by differences in location and local time. In addition, it is possibly due to the measurement methods used with different spatial and temporal resolutions.

[6] The above investigations are mostly concentrated on case studies with various data sets (e.g., ISR, ionosonde, GPS measurements) and provide some information about the behavior of the F2 layer during a special eclipse. Different from the previous studies, this paper studies the local time and solar zenith angle, solar cycle, dip angle, and background hmF2 effects on the ionospheric responses to a solar eclipse, on the basis of some case controlled simulations.

2. Ionospheric Observations

[7] To analyze the middle latitude F2-layer response to solar eclipses, we select ionosonde data during seven eclipse events when the path of the Moon's shadow passed through middle latitude with magnetic latitude larger than 30°. Furthermore, to ensure that the decrease in electron concentration because of the eclipse was large in comparison with the background ionospheric variability, we only considered those observatories with the obscuration at 200 km lager than 50%. The general information of these stations is listed in Table 1. The relative change in *foF*2, *rfoF*2, is defined as the ratio of the *foF*2 at eclipse time to that on the control day, which is the mean value of *foF*2 of the twenty days before and after the eclipse day. The smallest *rfoF*2 corresponds to the largest negative response of the F2 layer. So the smallest value of *rfoF*2 is used to describe the F2 layer response to an eclipse. All of the 23 stations during the corresponding eclipse events lie in the partial eclipse region and the largest obscuration at these stations varies from 51% to 99% (as listed in Table 1). For the sake of convenient comparison, the value of *rfoF*2 in the partial eclipse region, $rfoF2_P$, should be converted into a new value of *rfoF*2 at eclipse totality phase, $rfoF2_T$. Under the same geophysical conditions, the change in *foF*2 is assumed to be proportional to the masked percentage of solar radiation. Thus the equation for the conversion can be written as follows:

$$rfoF2_T = 1 - \frac{1 - rfoF2_P}{\Delta SP} \tag{1}$$

where ΔSP is the maximum obscuration as shown in Table 1. On the basis of these converted data, we plotted the local time and dip angle dependences of *rfoF*2 in Figures 1a and 1b, respectively. As shown in Figure 1a, there is a large local time effect on *rfoF*2: the relative change in *foF*2 is larger in the midday than in the morning and in the afternoon. Figure 1b shows that *rfoF*2 increases with respect

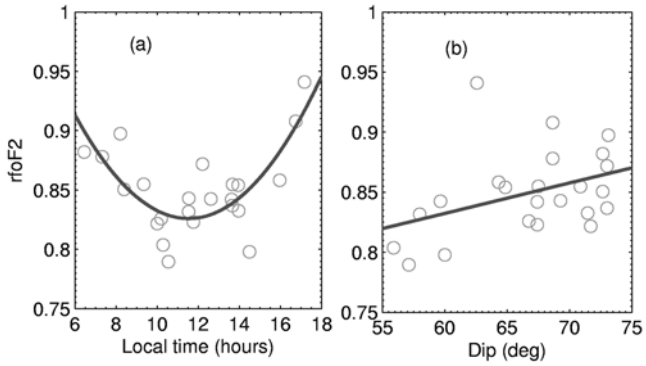

Figure 1. Scatterplots of rfoF2 versus (a) local time and (b) magnetic dip. The solid lines represent least squares regression lines. The data are from the selected 23 ionosonde stations.

to dip angle. That is, the larger dip angle causes the smaller decrease in *foF*2.

3. Ionospheric Model

[8] On the basis of previous works [*Zhang et al.*, 1993; *Tu et al.*, 1997; *Liu et al.*, 1999; *Lei et al.*, 2004a, 2004b], we develop a midlatitude and low-latitude theoretical ionospheric model, named as: Theoretical Ionospheric Model of the Earth in Institute of Geology and Geophysics, Chinese Academy of Sciences (TIME-IGGCAS) [*Yue et al.*, 2008]. This model adopts an eccentric dipole approximation to the Earth's magnetic field. It solves the coupled equations of the mass continuity, momentum, and energy of three main ions O^+, H^+ and He^+ in closed geomagnetic tubes with their foot points anchored at about 100 km altitude to yield values of concentrations, temperature, and field-aligned diffusion velocities of these three main ions as well as electrons. The model also calculates the values of concentrations of three minor ions N_2^+, O_2^+ and NO^+ in the F region under the assumption of photochemical equilibrium.

[9] The production rates of ions include the photoionization rates and chemical reaction production rates. The solar EUV radiation spectrum reported by *Richards et al.* [1994] is used to calculate the photoionization rates of neutral gas O_2, N_2 and O. The secondary ionization effect of daytime photoelectron and several nighttime ionization sources are also considered in the model. The loss rates of ions include chemical reaction losses and ion recombination losses. In the model 20 chemical reactions are considered. A detailed description of chemical reactions and their reaction coefficient and collision frequencies can be found in the work of *Lei et al.* [2004a].

[10] In this model the differences between the temperatures of different ions are ignored. We only calculate the O^+ temperature. The heating source for electrons considered includes photoelectron heating, elastic collision with neutral particles (N_2, O_2 and O), vibrational and rotational excitation of N_2 and O_2, excitation of the fine structure levels of atomic oxygen, excitation from 3P to 1D state for atomic oxygen, and the energy transfer by electron-ion collisions; for the O^+, ion-electron collisions, ion-ion collisions and elastic and inelastic collisions with the neutrals are considered. For the lower boundary, O^+ temperature equals to neutral temperature and electron's temperature is obtained under the heat equilibrium assumption. The energy equations of electron and O^+ are solved by the same finite difference method as that of mass continuity equation [*Lei*, 2005]. The reader is referred to the paper of *Lei* [2005] for detailed description of above mentioned heating rates. The photoelectron heating effect is similar to that of *Millward* [1993].

[11] The neutral temperature and densities are taken from the NRLMSIS-00 model [*Picone et al.*, 2002], and NO concentration is calculated from an empirical model developed by *Titheridge* [1997]. The neutral winds are determined by the HWM-93 model [*Hedin et al.*, 1996]. The previous measurements and modeling studies [e.g., *Roble et al.*, 1986; *Salah et al.*, 1986; *Müller-Wodarg et al.*, 1998; *Korenkov et al.*, 2003b] showed that during most of the eclipses events there is a slight decrease of no more than 60 K in the exospheric temperature and also a slight decrease in neutral concentration. In this study, we do not consider the possible effects of solar eclipse on neutral atmospheric compositions and temperature as well as neutral wind velocities. In this study, the simulations were carried out on a magnetic plane (n_p, n_l) (n_p = 201, n_l = 100) where n_p is the number of points along a magnetic field line, n_l is the number of magnetic field lines, with a time step of 60 seconds.

4. Solar Radiation During an Eclipse

[12] During a solar eclipse, the solar radiation reaching the top of the Earth atmosphere decreases a lot because the Sun is obscured by the Moon. To model the eclipse effects, the spectrum of solar radiation should be multiplied by an eclipse factor F(UT, h, Φ, θ). UT is the universal time, h the altitude, Φ the geographic longitude, and θ the geographic latitude.

[13] There are some studies on the ionospheric response to solar eclipses on the basis of numerical simulations in the past [e.g., *Stubbe*, 1970; *Roble et al.*, 1986; *Müller-Wodarg et al.*, 1998; *Boitman et al.*, 1999; *Liu et al.*, 1999; *Korenkov et al.*, 2003a, 2003b]. However, for the variations of solar radiation during a solar eclipse, they only considered the occultation of the photosphere by the moon. That is, in their simulations the value of F(UT, h, Φ, θ) is defined as the unmasked fraction of the area of the Sun's photosphere. Thus there would be no solar radiation reaching the earth atmosphere if the photosphere is totally obscured. However it is well known that some of the solar soft-X-ray and EUV radiation which originates from the solar corona is not obscured during a solar eclipse [*Rishbeth*, 1968; *Marriott et al.*, 1972; *Davis et al.*, 2000, 2001; *Curto et al.*, 2006]. *Davis et al.* [2000] presented a method for the first time to estimate the percentage of the solar ionizing radiation which remains unobscured during the eclipse by comparing the variation of the ionospheric E-layer with the observed behaviors during a control day and found that the flux of solar ionizing radiation fell to a minimum of 25 ± 2% of the value before and after the eclipse for the 11 August 1999 eclipse. Following a similar approach as *Davis et al.* [2000], *Curto et al.* [2006] evaluated the contribution of the radiation from different parts of the Sun in the Earth's

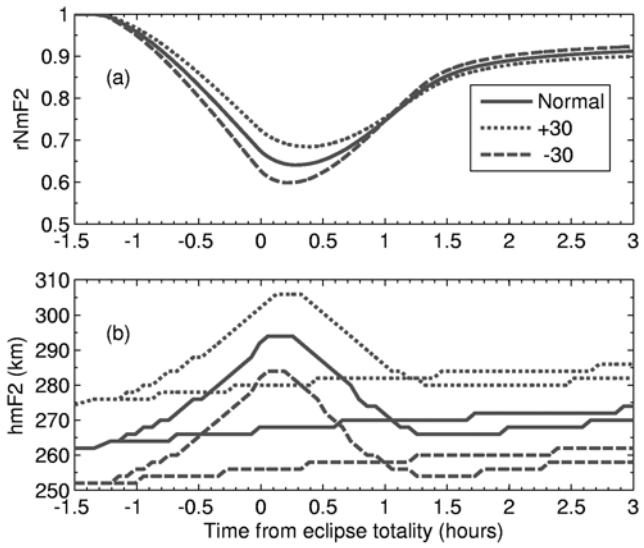

Figure 2. (a) Time variations in the simulated rNmF2, solid line for normal wind, dotted line for the wind by adding +30 m/s (equatorward), and dashed line for the wind by adding −30 m/s (polarward). (b) Time variations in the simulated hmF2: solid line for normal wind, dotted line for the wind by adding +30 m/s, and dashed line for the wind by adding −30 m/s, the lower line at totality for noneclipse and the higher one for eclipse. The zero in the *x* axes indicates the time of the totality.

ionosphere by using *foE* (critical frequency of E layer) data from many ionosonde stations and constructed an astronomical model to forecast the ionizing flux during the 11 August 1999 eclipse. The computation from the astronomical model shows that about 22 % of the radiation was unmasked at totality for that eclipse event, which is in accord with the result of *Davis et al.* [2000]. In this study, we define a revised eclipse factor F_R(UT, h, Φ, θ), the ratio of the unmasked solar radiation to the total solar radiation, which actually is representative of the percentage of the unmasked solar radiation at a given time (UT) and location (h, Φ, θ). This solar ionizing radiation includes the radiation originating both in the photosphere and in the corona. To calculate the value of the F_R(UT, h, Φ, θ), we first calculate the eclipse magnitude, defined as the fraction of the Sun's diameter occulted by the Moon, at a given location and time by a JavaScript Eclipse Calculator which is a Java program developed by Chris O'Byrne and Stephen McCann with the open source code on the web site (http://www.chris.obyrne.com/Eclipses/calculator.html). When the eclipse magnitude at any moment and any location is known, according to the astronomical model of *Curto et al.* [2006], we can calculate the F_R(UT, h, Φ, θ) at the corresponding time and location.

[14] For each simulation, initially we ran the model with the revised eclipse factor F_R(UT, h, Φ, θ) described above; and then ran the model again for identical conditions but excluding the eclipse shadow to identify the effects of the eclipse. *Davis et al.* [2001] showed a wide variety of values of the unobscured solar ionizing radiation for eclipses over seventy years from 1932 to 1999. In our study, we focus on the theoretical analysis of the effects of some parameters on the ionospheric response to an eclipse, so an identical value of the unobscured solar radiation will be more convenient. We assume an identical value of the unobscured solar ionizing radiation at totality of 22%, the same as that of the 11 August 1999 eclipse.

5. Case Control Studies

[15] In this section, we carry out four case controlled studies to study the background hmF2 effects, local time and solar zenith angle effects, solar cycle effects, and dip angle effects, respectively. In the following sections of the paper we use the symbols *rNmF*2, *rhmF*2, *rNe*, *rTe*, and *rPf* to denote the relative changes induced by a solar eclipse in the *NmF*2, *hmF*2, *Ne* (electron concentration), *Te* (electron temperature) and *Pf* (plasma diffusion flux), respectively. The change in *NmF*2, *rNmF*2, is defined as $NmF2_E/NmF2_C$. The change in *hmF*2, *rhmF*2, is defined as $hmF2_E$-$hmF2_C$. The change in *Ne*, *rNe*, is defined as Ne_E/Ne_C. The change in *Te*, *rTe*, is defined as Te_E-Te_C. The change in *Pf*, *rPf*, is defined as Pf_E-Pf_C. The subscripts E and C denote the situation on the eclipse day and the control day, respectively. In addition, we define τ as the delay time of the minimum value of rNmF2 with respect to the eclipse totality phase.

5.1. Effect of Background hmF2

[16] For case 1, we performed three simulations using the variation in solar radiation of the 31 July 1981 total eclipse to study the effect of background *hmF*2 on the F2 layer response to a solar eclipse. The simulation is made at geographic longitude 127°E. On this plane, the total eclipse occurred at around 54.5°N, and the totality was at 12 LT. The solar activity index F107 was set to 140. The only difference among these simulations is in the neutral wind. One used empirical model HWM93 (called normal), the other two also used HWM93 but adding a horizontal wind of +30 m/s and −30 m/s (equatorward is positive), respectively.

[17] Figure 2 illustrates the *rNmF*2, the background *hmF*2 (without eclipse) and the *hmF*2 during the solar eclipse. One can see from Figure 2 that because of an added equatorward wind the background *hmF*2 was lifted by around 12 km and because of an added polarward wind the background *hmF*2 was lowered around 12 km. The simulations also show that an added equatorward wind causes a larger *rNmF*2 with the value of *rNmF*2 from 0.64 to 0.685 and an added polarward wind causes a smaller *rNmF*2 with the value of *rNmF*2 from 0.64 to 0.6 (as shown in Figure 2a). The results show that the higher the background *hmF*2 is, the larger the *rNmF*2 is, corresponding to the smaller F2 layer electron concentration response. The simulated results also show that for the altitudes above 200 km, *rNe* is smaller at lower altitude. So the higher *hmF*2 results in the larger *rNmF*2. In addition, there are little differences in the temporal and spatial evolutions of the *rNe* between these simulations. An interesting result about Figure 2 is that *hmF*2 reaches its equilibrium height 10 minutes earlier when starting with a lower *hmF*2. During the recovery phase (from the totality to the end of an eclipse), the electron concentration increases faster at lower heights, which causes *hmF*2 to drop gradu-

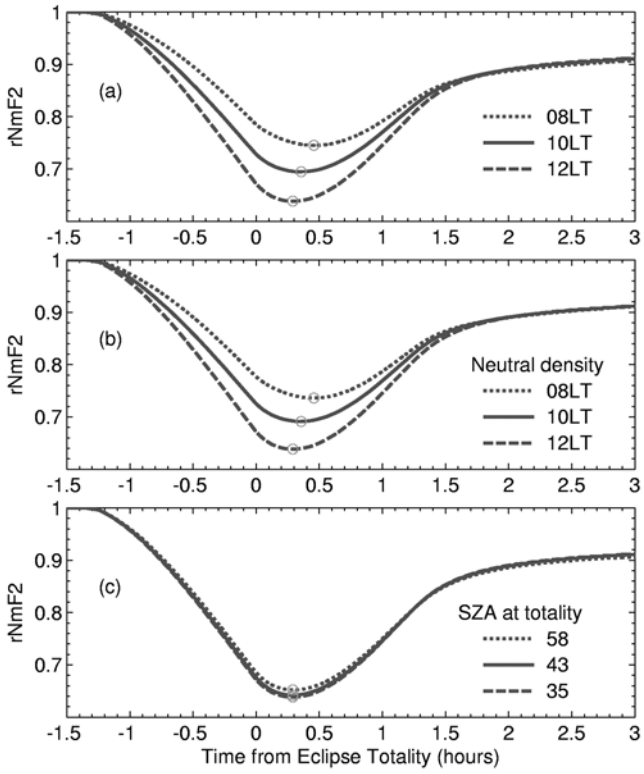

Figure 3. (a) Temporal evolutions of the simulated rNmF2 with the totality at 08 LT (SZA = 58) (dotted line), 10 LT (SZA = 43) (solid line), and 12 LT (SZA = 35) (dashed line), respectively. (b) Temporal evolutions of the simulated rNmF2 with the neutral concentration at 08, 10, and 12 LT, respectively, but with the same SZA (35°). (c) Temporal evolutions of the simulated rNmF2 with the SZA at totality equal to 58°, 43°, and 35°, respectively, but with the same neutral concentration at 12 LT. The zero in the x axes indicates the time of totality. The three circles in each denote the smallest rNmF2.

ally. The *hmF*2 would reach its equilibrium height at some time before the end of the eclipse and continually drop until the end of the eclipse. Because a complete recovery of the F2 layer will take a few hours so the *hmF*2 will lower than equilibrium height for several hours (as shown in Figure 2b).

5.2. Local Time and Solar Zenith Angle Effects

[18] For case 2, we performed three simulations using the variation in solar radiation of the 31 July 1981 total eclipse to study the local time dependence of the eclipse effect in the F2 layer. The following geophysical parameters are adopted: DOY (day of year) = 210, F10.7 = 140, F10.7A = 140, geomagnetic index ap = 5. We simulated the eclipses at different LT. The times of the totality were 08 LT (SZA ≈ 58°), 10 LT (SZA ≈ 43°), and 12 LT (SZA ≈ 35°), respectively. So the different local time of the eclipse totality is the main difference among these simulations.

[19] Figure 3a illustrates the temporal evolutions of the simulated *rNmF*2 with eclipse totality at 08 LT, 10 LT, and 12 LT, respectively. Figure 4 illustrates the temporal and spatial evolutions of the simulated *rNe* of these simulations. Figure 3a shows that the smallest *rNmF*2 for the 08 LT, 10 LT and 12 LT eclipse are 0.74, 0.69, and 0.64, respectively; and the values of τ are 26 minutes, 21 minutes, and 17 minutes, respectively. The simulated results are consistent with the measurements (shown as Figure 1a): the decrease in *NmF*2 is larger in the midday than in the morning. From Figure 4 we can see that for the E and F1 region (altitudes below 200 km) there is little difference between the variations in *Ne* at various local times; whereas for the F region between 200 km and 400 km, the value of *rNe* is largest at 08 LT and smallest at 12 LT.

[20] As is known, there are variations in the neutral concentration and in solar zenith angle at different local time. To ensure which one is the main contributor to the local time effect, we carried out two other simulations to investigate the neutral concentration effect and the solar zenith angle effect. When the neutral concentration effect is investigated, the solar zenith angle is the same as that at 12 LT. When the solar zenith angle is investigated, the neutral concentration is the same as that at 12 LT.

[21] Figures 3b and 3c illustrate the results of the neutral concentration effect and the solar zenith angle effect, respectively. It should be noted that in these simulations the neutral concentration is largest at 12 LT and smallest at 08 LT. Figure 3b shows that a larger neutral concentration causes a larger decrease in NmF2. Figure 3c shows that there is almost the same change in *NmF*2 for various solar zenith angles. That is, the local time effect of the eclipse is mainly contributed from the difference in the neutral concentration. From Figure 3b, one can also find that the difference in the delay time τ is caused by the difference in the neutral concentration. For the delay time τ, it is now well known that it is related with the "sluggishness" of the ionosphere [*Appleton*, 1953; *Rishbeth*, 1968; *Rishbeth and Garriott*, 1969]. It means that changes of *Ne* should theoretically lag behind changes in electron production rate

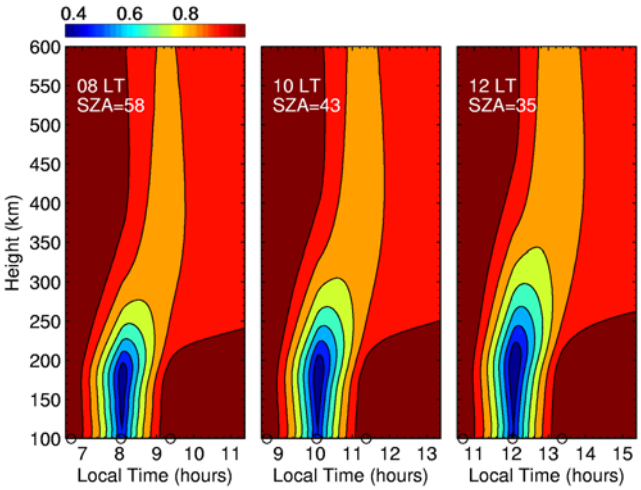

Figure 4. The temporal and spatial evolutions of the simulated rNe with the totality at 08, 10, and 12 LT, respectively. Text in each panel indicates the time of totality and the corresponding solar zenith angle. Three circles in each panel indicate the beginning, totality, and end of the eclipse, respectively.

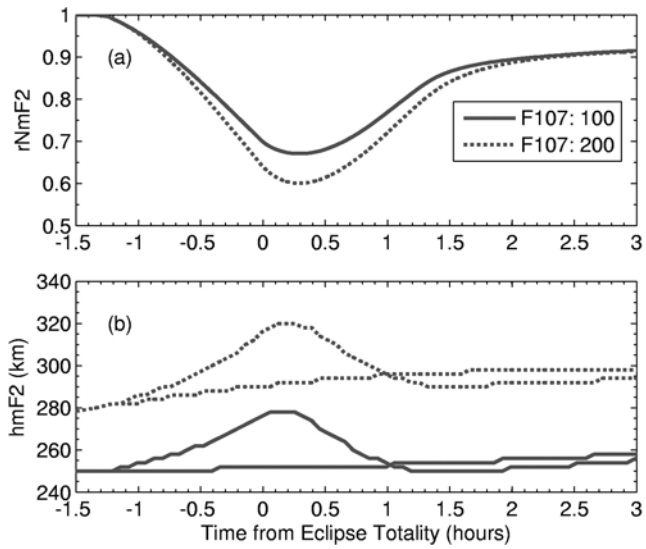

Figure 5. (a) Time variations in the simulated rNmF2, solid line for F107 = 100 and dotted line for F107 = 200. (b) Time variations in the simulated hmF2: solid lines for F107 = 100 and dotted lines for F107 = 200, the lower line at totality for noneclipse and the higher one for eclipse. The zero in the x axes indicates the time of the totality.

by a time constant of $1/2\alpha Ne$ for low altitudes and $1/\beta$ for high altitudes, where α is the square law loss coefficient and β is the linear loss coefficient. At the height of *hmF*2, β is proportional to $[N_2]$ (molecular N_2 concentration). The larger $[N_2]$ at 12 LT causes a larger β, which thus results in a smaller value of τ. The simulations also show that the largest response of *hmF*2 (not shown) occurs at 12 LT eclipse with *rhmF*2 of ~26 km and the smallest one occurs at 08 LT eclipse with *rhmF*2 of ~18 km. The simulated results also show that there is a larger decrease in electron temperature (not shown) for the 12 LT eclipse than that for the 08 LT eclipse.

5.3. Solar Cycle Effects

[22] For case 3, we performed two simulations using the variation in solar radiation of the 31 July 1981 total eclipse to study the solar activity dependence of the eclipse effect in the F2 layer. The solar activity indexes F107 for the two simulations were set as 100.0 and 200.0, respectively. The geographic plane for the two simulations is at 105°E and the total eclipse occurred at 53.8°N with the time of the totality at 12 LT.

[23] Figure 5a illustrates the temporal evolutions of the simulated *rNmF*2 at low solar activity and high solar activity, respectively, and Figure 5b shows the corresponding variations of the background *hmF*2 (without eclipse) and the *hmF*2 during the eclipse at these two solar activity conditions. The temporal and spatial evolutions of the simulated *rNe* at low solar activity F107 = 100 and at high solar activity F107 = 200 are illustrated in Figures 6a and 6b, respectively. As shown in Figure 5a, the smallest values of *rNmF*2 for solar activity index F107 = 200 and F107 = 100 are 0.6 and 0.67, respectively, which means that the lager solar activity causes the larger variations in *NmF*2. Figure 5a also shows the same delay time τ in the two simulations. Figure 5b shows that the background hmF2 is higher by about 40 km at F107 = 200 than at F107 = 100, whereas the change in *hmF*2 is identical with the largest *rhmF*2 of about 28 km for both simulations. As illustrated in Figure 6, there are much larger decreases in electron concentration in the F2 region at high-solar-activity conditions than at low-solar-activity condition. The larger eclipse effect at high solar activity also expands to the

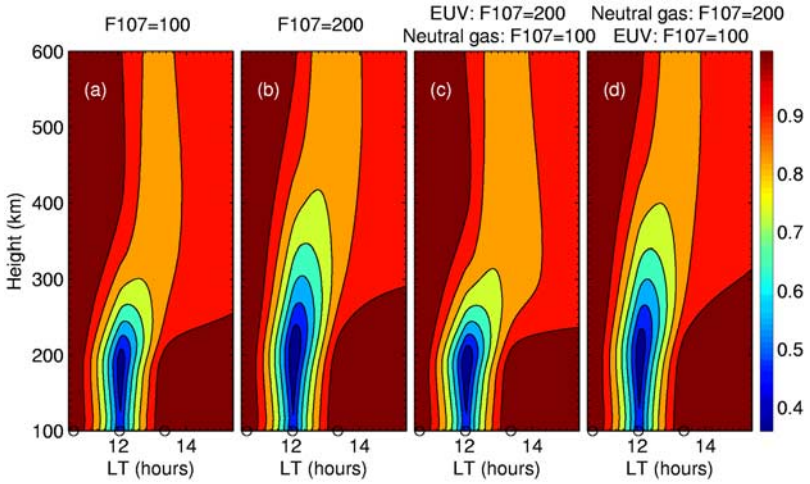

Figure 6. Temporal and spatial evolutions of the simulated rNe at (a) low solar activity F107 = 100 and (b) high solar activity F107 = 200. The right two panels are similar to the left two ones but use different solar activity index to calculate solar EUV radiation and neutral gas concentrations: (c) solar EUV radiation at low solar activity of F107 = 100 and neutral gas concentrations at high solar activity of F107 = 200 and (d) solar EUV radiation at high solar activity of F107 = 200 and neutral gas concentrations at low solar activity of F107 = 100. Three circles in each panel indicate the time of eclipse, begin, totality, and end, respectively.

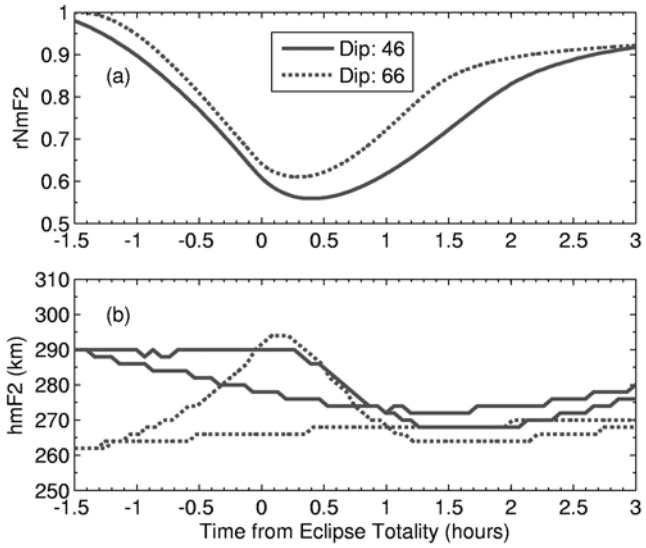

Figure 7. (a) Time variations in the simulated rNmF2: solid line for a location with dip = 46° and dotted line for a location with dip = 66°. (b) Time variations in the simulated hmF2: solid lines for dip = 46° and dotted lines for dip = 66°, the lower line at totality for noneclipse and the higher one for eclipse. The zero in the *x* axes indicates the time of the totality.

lower F region. The simulated results show that for the low solar activity of F107 = 100, the largest decrease in electron concentration occurs at an altitude of about 182 km with a value of *rNe* = 0.386; whereas for the high solar activity of F107 = 200, the largest decrease in electron concentration occurs at an higher altitude of about 200 km with a smaller value of *rNe* = 0.362. As shown in Figure 5b, the background hmF2 rises nearly 40 km at high solar activity F107 = 200 compared with that at low solar activity F107 = 100. According to the result of the control case 1 discussed above, the much higher background hmF2 at F107 = 200 should result in the larger *rNmF*2, whereas the contrary result as shown in Figure 5a shows that the effect of the much larger decreases in electron concentration over all altitudes of F region exceeds that of the higher background hmF2, which results in the smaller *rNmF*2 at high solar activity.

[24] As is known, both solar EUV radiation and the neutral gas concentration vary with solar activity level [*Balan et al.*, 1994; *Liu et al.*, 2003; *Liu et al.*, 2006]. In order to make clear which one is the dominant factor for the different eclipse effects at low- and high-solar-activity condition, we carried out other two simulations: for one simulation, we used EUVAC [*Richards et al.*, 1994] with F107 = 200 to calculate solar EUV radiation and used NRLMSIS-00 [*Picone et al.*, 2002] with F107 = 100 to calculate neutral gas concentration; for the other, we used EUVAC with F107 = 100 to calculate solar EUV radiation and used NRLMSIS-00 with F107 = 200 to calculate neutral gas concentration.

[25] Figure 6 shows the temporal and spatial evolutions of the simulated *rNe* at four different conditions: first, solar activity F107 = 100 is used to calculate both solar EUV radiation and neutral gas concentration; second, F107 = 200 is used to calculate solar EUV radiation and F107 = 100 is used to calculate neutral gas concentration; third, F107 = 100 is used to calculate solar EUV radiation and F107 = 200 is used to calculate neutral gas concentration; fourth, solar activity F107 = 200 is used to calculate both solar EUV radiation and neutral gas concentration. As illustrated in Figure 6, there is very small difference between the first and the third panels and also very small difference between the second and the fourth panels. The small difference between Figures 6a and 6c indicates that the variation in solar EUV radiation flux is not a main contributor for the large difference of F region responses to a solar eclipse at low solar activity and at high solar activity. On the contrary, the large difference between Figures 6b and 6c (or between Figures 6a and 6d) shows that the variation in neutral gas densities is the major contributor for the large difference of the F region responses to a solar eclipse at low solar activity and high solar activity. In conclusion, the background neutral gas has an important effect on the F2 layer responses to a solar eclipse.

5.4. Dip Angle Effects

[26] For case 4, we performed two simulations using the variations in solar radiation of the 29 April 1976 total eclipse and of the 11 August 1999 total eclipse to study the magnetic dip dependence of the eclipse effect in the F2 layer. The solar activity index F107 was set to 180.0 for two simulations. The geographic plane simulated for two simulations is taken at 15°E and 9°E, respectively. As for these two planes, the total eclipse occurred at 32.3°N with dip = 46°and 49.1°N with dip = 66°, respectively; and the times of the eclipse totality were 1112 LT and 1109 LT, respectively. The neutral concentration during the eclipse in these two simulations has been adjusted to be the same. So the main difference between the two simulations is induced by the magnitude of dip.

[27] Figure 7a illustrates the temporal evolutions of the simulated *rNmF*2 at dip = 46° and dip = 66°, respectively, and Figure 7b shows the corresponding variations of the background *hmF*2 (without eclipse) and the *hmF*2 during the eclipse. The temporal and spatial evolutions of the simulated *rNe* at dip = 46° and dip = 66° are illustrated in Figures 8a and 8b, respectively. Figure 7a shows that the decrease in NmF2 at dip = 66° is smaller than that at dip = 46°. The simulated results are consistent with the observed results (shown in Figure 1b): the larger value of dip results in the smaller change in NmF2 or foF2. Figure 7b shows that the background hmF2 is lower at dip = 66° than at dip = 46°, whereas the change in hmF2 is larger at dip = 66° than at dip = 46°. According to the result of control case 1 discussed above, the lower background *hmF*2 should result in the smaller *rNmF*2, whereas the contrary result as shown in Figure 7a shows that the effects of dip exceeds that of the background *hmF*2.

[28] Figure 8 shows the larger *rNe* at the larger dip for the altitudes above 250 m, which might be caused by the larger downward ion flux at the larger dip as illustrated in Figures 8c and 8d. The eclipse can cause a rapid lowering of electron temperature and a subsequent change in the diffusive equilibrium-scale height; therefore it results in ionizations moving downward from the plasmasphere. To better

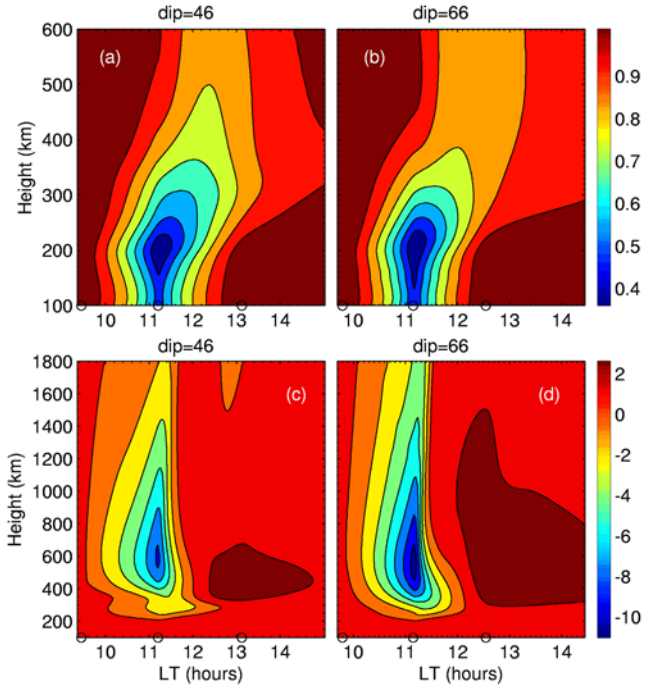

Figure 8. Temporal and spatial evolutions of the simulated rNe at a location with (a) dip = 46° and (b) dip = 66°. The temporal and spatial evolutions of the simulated variation in plasma diffusion flux, rPf, at a location with (c) dip = 46° and (d) dip = 66°. It is in unit of 10^{12} $m^{-2}s^{-1}$. Three circles in each indicate the beginning, totality, and end of the eclipse, respectively.

understand the role of the change in temperature and the role of dip, we carried out two simulations for dip = 46 and dip = 66 by running the model with no change in temperature. The simulated results show almost the same ionospheric response in these two simulations. Also, there is almost no difference in ionization flux between the control day and the eclipse day in both of the two simulations because there is no change in temperature. Comparing the results with change in temperature and without change in temperature, we can find that decrease in electron temperature results in ionizations moving downward from the top of ionosphere. Furthermore, Figures 8c and 8d show that a larger value of dip causes a larger downward diffusion flux, which results in the smaller changes in electron concentration in the F region (as shown in Figure 8b). The effect of the dip (I) is to control the rate of diffusion according to $\sin^2 I$. So the larger dip causes the larger downward diffusion flux (as shown in Figure 8d).

6. Discussion

[29] The ionosphere at low heights (the E and F1 regions) is mainly dominated by the photochemical processes which cause the ionospheric response to an eclipse at these heights is determined by the variation in solar radiation. Whereas regarding the F2 region, it is controlled mainly by the transport processes, so the eclipse effect in this region is not only related to the change in solar radiation, but also related to the background parameters such as background *hmF*2, local time, solar activity, and magnetic dip. As for the heights above the F1 layer in the middle latitude ionosphere, the variations in electron concentration are larger at lower heights during solar eclipse. Therefore the higher *hmF*2 will yield the smaller eclipse effect in the F2 layer. As modeled in control case 1, the temporal and spatial evolution of *rNe* change very slightly when the horizontal neutral winds are altered by adding a horizontal equatorward wind of 30 m/s. That is, the *rNe* at a fixed height are affected slightly by the altered neutral winds. Therefore neutral winds affect the F2-layer response to an eclipse mainly by uplifting or dropping the F2-layer peak height. Local time or SZA is also one of the control factors for the eclipse effect in the F region. Both the measurements and simulations (in control case 2) show that the eclipse effect in the early morning is much smaller than that at midday.

[30] In the F2 region, the continuity equation for the electron concentration Ne as function of time t is

$$\partial Ne/\partial t = q - \beta \cdot Ne - \nabla \cdot (NeV) \tag{2}$$

Where q is the rate of production of electrons, β is the loss coefficient, and V is the plasma velocity (positive upwards). We solve equation (2) by assuming an eclipse function $q = q_0 * \cos(\chi) * \exp(-at)$ and make the divergence of the flux constant, where q_0 is the rate of production of electrons with solar zenith angle $\chi = 0°$ and a = constant. Thus we obtain the electron concentration Ne_E on the eclipse day:

$$Ne_E = \frac{q_0 \cos(\chi)}{\beta - a}(\exp(-at) + k \cdot \exp(-\beta t)) \tag{3}$$

The k in equation (3) is a positive constant. For the electron concentration Ne_C on the control day, we can obtain Ne_C by making the limit of a be zero:

$$Ne_C = \frac{q_0 \cos(\chi)}{\beta}(1 + k \cdot \exp(-\beta t)) \tag{4}$$

Comparing equation (3) with equation (4), we can obtain the relative change in electron concentration, *rNe*:

$$rNe = \left(1 + \frac{a}{\beta - a}\right) \cdot \left(\exp(-at) + \frac{(1 - \exp(-at)) \cdot k}{\exp(\beta t) + k}\right) \tag{5}$$

According to equation (5), one can find that the solar zenith angle has no effect on the ionospheric response to an eclipse because solar zenith angle has the same effect on the electron concentration on the control day and the eclipse day (as shown in equations (3) and (4)). However, from equation (5), we can find that the loss coefficient β have a significant effect on the ionospheric response: a larger β causes a smaller value of *rNe* which means a larger decrease in *Ne*. The loss coefficient β is directly proportional to the concentrations of neutral molecular gases N_2 and O_2: $\beta = \gamma_1[N_2] + \gamma_2[O_2]$, where γ_1 and γ_2 are the chemical reaction coefficients. So a larger neutral concentration will cause a larger value of β and therefore results a smaller value of *rNe*.

[31] As modeled in controlled case 3, the eclipse effect in the F region varies with the solar activity level, which is

larger at high solar activity than at low solar activity. The simulated results show the discrepancy of the ionospheric response is not caused by the difference of solar EUV radiation at high and low solar activity, but by the difference of the background neutral concentration between high solar activity and low solar activity. As is known, the rate of production of electrons q_0 is directly proportion to solar EUV flux. Solar EUV flux have the same effect on both Ne_C and Ne_E as shown in equations (3) and (4), which results that solar EUV flux has little or even no effect on the ionospheric response to an eclipse if there is little or no change in EUV flux between the eclipse and control days. On the contrary, the neutral concentration has a significant effect on the ionospheric response to an eclipse, which has discussed in the previous paragraph.

[32] As simulated in controlled case 4, magnetic dip has a large effect on the ionospheric response to an eclipse. The larger dip causes the larger downward diffusion flux which results in the smaller changes in electron concentration in the F region as shown in Figure 8. On the basis of several eclipse measurements, *Evans* [1965b] suggested that the increase in *foF*2 might be caused by the large downward diffusion of ionization from above hmF2. As discussed in case 1, 2, and 3, the high background *hmF*2, the small solar zenith angle, and the low solar activity are helpful to yield the smaller decrease in *Ne*. Using these conditions, we modeled again the ionospheric response to an eclipse at a location with the dip larger than 75, but still did not obtain a result of an increase in *foF*2. It should be noted that in this study we do not consider the possible effects of the solar eclipse on neutral atmospheric composition and temperature as well as neutral wind velocities. *Müller-Wodarg et al.* [1998] used the Coupled Thermosphere Ionosphere Plasmasphere model (CTIP) [*Millward et al.*, 1996] to model the eclipse effect in the ionosphere and thermosphere during a solar eclipse and found an enhancement of *NmF*2 during and after the eclipse. Simulated results showed that the increase in *NmF*2 is caused by the atmosphere's contraction during the eclipse and by the increased $[O]/[N_2]$ ratio after the eclipse. By Global Self-Consistent Model of the Thermosphere-Ionosphere and Protonsphere (GSM-TIP), *Korenkov et al.* [2003b] also investigated the effects of a solar eclipse on the upper atmosphere and found an increase in *foF*2 after the eclipse. Their results suggested this increase was mainly caused by the decrease in molecular gas N_2 concentrations. Both of the studies mentioned above show that the perturbation in the neutral gas temperature and densities is the main reason for the behavior of increased *NmF*2, though their results are not completely identical. Our results also indirectly show that the plasma diffusion from higher altitudes considered alone is not enough for the increase in *NmF*2 and the perturbation in the neutral gas might be needed.

7. Summary

[33] In this study, we statistically analyzed the solar zenith angle and magnetic dip dependence of the change in *foF*2 during solar eclipses with the data derived from 23 ionosonde stations during seven eclipse events. The statistical results show that the decrease in *foF*2 has local time dependence that it is larger in the midday than in the morning and afternoon. The statistical results also show a magnetic dip effect that the decrease in *foF*2 decreases with increasing dip. Then, to model the eclipse effects of the ionosphere, according to the astronomical model of *Curto et al.* [2006], we construct a solar spectrum model for solar eclipses by introducing a revised eclipse factor $F_R(UT, h, \Phi, \theta)$, which is equal to the ratio of the unmasked solar radiation to the total solar radiation, taking account of the radiation from the solar corona when calculating the total solar radiation. Because of the combined control of the photochemical process and the plasma transport process, the eclipse effect in the F2 region is more complicated, which might be related to background peak height of F2 layer, local time, solar activity, and magnetic dip. To make clear how these physical parameters affect the F2 layer response to an eclipse, these four parameters are employed in the control case studies by using a midlatitude and low-latitude theoretical ionospheric model. Furthermore, the solar zenith angle effect and the neutral concentration effect are investigated, respectively, to analysis the local time effect. Also, the solar EUV flux effect and neutral concentration effect also investigated, respectively, to analyze the difference response to an eclipse at low solar activity and high solar activity. The central finding of this paper is that most of the observed differences in behavior of NmF2 during eclipses can be attributed to differences in O^+ loss rate brought about by the background differences in the neutral molecular densities. The main simulated results are summarized as follows:

[34] 1. The higher background hmF2 causes the larger *rNmF2*, corresponding to the smaller decrease in the F2 layer electron concentration.

[35] 2. The eclipse effect in the F region has evident local time dependence: the F2 layer response is larger in the midday than in the morning and afternoon. The local time effect is mostly contributed from the difference in the neutral concentration.

[36] 3. At high solar activity or low solar activity, the background solar radiation before and after an eclipse very slightly affects the F2 layer response to an eclipse; whereas the neutral gas concentrations have a significant contributor to the eclipse effect in the F2 region: the larger neutral gas concentrations at high solar activity cause a corresponding larger ionospheric response to a solar eclipse.

[37] 4. The dip has a large effect on the ionospheric response to a solar eclipse. The larger dip causes the larger downward diffusion flux which makes up the ion losses and subsequently results in the smaller changes in electron concentration in the F region. The simulated results are consistent with the measurements.

[38] **Acknowledgments.** The authors wish to express gratitude to referee Dr. Phil Richards for pointing out the importance of neutral density to the interpretation of the measurements and to another referee for insightful comments. The authors also thank the Space Physics Interactive Data Resource of the National Geophysical Data Center for supplying the ionospheric data. This research was supported by National Natural Science Foundation of China (40725014, 40674090, and 40636032) and National Important Basic Research Project (2006CB806306).

[39] Zuyin Pu thanks the reviewers for their assistance in evaluating this paper.

References

Adeniyi, J. O., S. M. Radicella, I. A. Adimula, A. A. Willoughby, O. A. Oladipo, and O. Olawepo (2007), Signature of the 29 March 2006 eclipse

on the ionosphere over an equatorial station, *J. Geophys. Res.*, *112*, A06314, doi:10.1029/2006JA012197.
Afraimovich, E. L., E. A. Kosogorov, and O. S. Lesyuta (2002), Effects of the August 11, 1999 total solar eclipse as deduced from total electron content measurements at the GPS network, *J. Atmos. Sol.-Terr. Phys.*, *64*, 1933–1941.
Afraimovich, E. L., K. S. Palamartchouk, N. P. Perevalova, V. V. Chemukhov, A. V. Lukhnev, and V. T. Zalutsky (1998), Ionospheric effects of the solar eclipse of March 9, 1997, as deduced from GPS data, *Geophys. Res. Lett.*, *25*(4), 465–468.
Appleton, E. V. (1953), A note on the "sluggishness" of ionosphere, *J. Atmos. Terr. Phys.*, *3*, 228–232.
Balan, N., G. J. Bailey, B. Jenkins, P. B. Rao, and R. J. Moffett (1994), Variations of ionospheric ionization and related solar fluxes during an intense solar cycle, *J. Geophys. Res.*, *99*(A2), 2243–2253.
Baran, L. W., I. I. Ephishov, I. I. Shagimuratov, V. P. Ivanov, and A. F. Lagovsky (2003), The response of the ionospheric total electron content to the solar eclipse on August 11, 1999, *Adv. Space Res.*, *31*(4), 989–994.
Boitman, O. N., A. D. Kalikhman, and A. V. Tashchilin (1999), The mid-latitude ionosphere during the total solar eclipse of March 9, 1997, *J. Geophys. Res.*, *104*(A12), 28,197–28,206.
Cheng, K., Y.-N. Huang, and S.-W. Chen (1992), Ionospheric effects of the solar eclipse of September 23, 1987, around the equatorial anomaly crest region, *J. Geophys. Res.*, *97*(A1), 103–111.
Cohen, E. A. (1984), The study of the effect of solar eclipses on the ionosphere based on satellite beacon observations, *Radio Sci.*, *19*(3), 769–777.
Curto, J. J., B. Heilig, and M. Pinol (2006), Modeling the geomagnetic effects caused by the solar eclipse of 11 August 1999, *J. Geophys. Res.*, *111*, A07312, doi:10.1029/2005JA011499.
Datta, S., P. Bandyopadhyay, and R. N. Datta (1959), Ionospheric observations on the F-region during the solar eclipse of 19 April 1958, *J. Atmos. Terr. Phys.*, *16*, 182–185.
Davis, C. J., M. Lockwood, S. A. Bell, J. A. Smith, and E. M. Clarke (2000), Ionospheric measurements of relative coronal brightness during the total solar eclipses of August 11, 1999 and July 9, 1945, *Ann. Geophys.*, *18*, 182–190.
Davis, C. J., E. M. Clarke, R. A. Bamford, M. Lockwood, and S. A. Bell (2001), Long term changes in EUV and X-ray emissions from the solar corona and chromosphere as measured by the response of the Earth's ionosphere during total solar eclipses from 1932 to 1999, *Ann. Geophys.*, *19*, 263–273.
Evans, J. V. (1965a), An *F* region eclipse, *J. Geophys. Res.*, *70*(1), 131–142.
Evans, J. V. (1965b), On the behavior of foF2 during solar eclipses, *J. Geophys. Res.*, *70*(3), 733–738.
Farges, T., J. C. Jodogne, R. Bamford, Y. Le Roux, F. Gauthier, P. M. Vila, D. Altadill, J. G. Sole, and G. Miro (2001), Disturbances of the western European ionosphere during the total solar eclipse of 11 August 1999 measured by a wide ionosonde and radar network, *J. Atmos. Sol.-Terr. Phys.*, *63*, 915–924.
Farges, T., A. Le Pichon, E. Blanc, S. Perez, and B. Alcoverro (2003), Response of the lower atmosphere and the ionosphere to the eclipse of August 11, 1999, *J. Atmos. Sol.-Terr. Phys.*, *65*, 717–726.
Hedin, A. E., E. L. Fleming, and A. H. Manson (1996), Empirical wind model for the upper, middle and lower atmosphere, *J. Atmos. Terr. Phys.*, *58*, 1421–1447.
Higgs, A. J. (1942), Ionospheric measurements made during the total solar eclipse of 1940, October 1, *Mon. Not. Roy. Astron. Soc.*, *102*, 24–34.
Huang, C. R., C. H. Liu, K. C. Yeh, K. H. Lin, W. H. Tsai, H. C. Yeh, and J. Y. Liu (1999), A study of tomographically reconstructed ionospheric images during a solar eclipse, *J. Geophys. Res.*, *104*(A1), 79–94.
Hunter, A. N., B. K. Holman, D. G. Fieldgate, and R. Kelleher (1974), Faraday rotation studies in Africa during the solar eclipse of June 30, 1973, *Nature*, *250*, 205–206.
Klobuchar, J. A., and H. E. Whitney (1965), Ionospheric electron content measurements during a solar Eclipse, *J. Geophys. Res.*, *70*(5), 1254–1257.
Korenkov, Y. N., V. V. Klimenko, V. Baran, I. I. Shagimuratov, and F. S. Bessarab (2003a), Model calculations of TEC over Europe during 11 August 1999 solar eclipse, *Adv. Space Res.*, *31*(4), 983–988.
Korenkov, Y. N., V. V. Klimenko, F. S. Bessarab, N. S. Nutsvalyan, and I. Stanislawska (2003b), Model/Data comparison of the F2-region parameters for the 11 August 1999 solar eclipse, *Adv. Space Res.*, *31*(4), 995–1000.
Le, H., L. Liu, X. Yue, and W. Wan (2008), The ionospheric responses to the 11 August 1999 solar eclipse: Observations and modeling, *Ann. Geophys.*, *26*, 107–116.
Lei, J. (2005), Statistical analysis and modeling investigation of middle latitude ionosphere, dissertation for the doctoral degree, pp. 1–121, Institute of Geology and Geophysics, Chinese Academy of Sciences, Beijing, China.
Lei, J., L. Liu, W. Wan, and S. R. Zhang (2004a), Modeling the behavior of ionosphere above Millstone Hill during the September 21–27, 1998 storm, *J. Atmos. Sol.-Terr. Phys.*, *66*, 1093–1102.
Lei, J., L. Liu, W. Wan, and S. R. Zhang (2004b), Model results for the ionospheric lower transition height over mid-latitude, *Ann. Geophys.*, *22*, 2037–2045.
Liu, L., W. Wan, J. N. Tu, Z. T. Bao, and C. K. Yeh (1999), Modeling study of the ionospheric effects during a total solar eclipse, *Chin. J. Geophys.*, *42*(3), 296–302.
Liu, J. Y., Y. I. Chen, and J. S. Lin (2003), Statistical investigation of the saturation effect in the ionospheric foF2 versus sunspot, solar radio noise, and solar EUV radiation, *J. Geophys. Res.*, *108*(A2), 1067, doi:10.1029/2001JA007543.
Liu, L., W. Wan, B. Ning, O. M. Pirog, and V. I. Kurkin (2006), Solar activity variations of the ionospheric peak electron density, *J. Geophys. Res.*, *111*, A08304, doi:10.1029/2006JA011598.
Marriott, R. T., D. E. St. John, R. M. Thorne, S. V. Venkateswaran, and P. Mahadevan (1972), Ionospheric effects of two recent solar eclipses, *J. Atmos. Terr. Phys.*, *34*, 695–712.
Millward, G. H. (1993), A global model of the earth's thermosphere, ionosphere and plasmasphere: Theoretical studies of the response to enhanced high-latitude convection, dissertation for the doctoral degree, pp. 1–195, Univ. of Sheffield, U.K.
Millward, G. H., R. J. Moett, S. Quegan, and T. J. Fuller-Rowell (1996), A coupled Thermosphere-Ionosphere-Plasmasphere Model (CTIP), in *Solar Terrestrial Energy Program: Handbook of Ionosphere Models*, edited by R. W. Schunk, pp. 239–279, Utah State University, Logan.
Müller-Wodarg, I. C. F., A. D. Aylward, and M. Lockwood (1998), Effects of a mid-latitude solar eclipse on the thermosphere and ionosphere—A modelling study, *Geophys. Res. Lett.*, *25*(20), 3787–3790.
Oliver, W. L., and S. A. Bowhill (1974), The F1 region during a solar eclipse, *Radio Sci.*, *9*(2), 185–195.
Picone, J. M., A. E. Hedin, D. P. Drob, and A. C. Aikin (2002), NRLMSISE-00 empirical model of the atmosphere: Statistical comparisons and scienti5c issues, *J. Geophys. Res.*, *107*(A12), 1468, doi:10.1029/2002JA009430.
Pierce, J. A. (1948), The ionospheric eclipse of October 1, 1940, *Proc. IRE.*, *36*, 137–144.
Richards, P. G., J. A. Fennelly, and D. G. Torr (1994), EUVAC: A Solar EUV Flux Model for Aeronomic Calculations, *J. Geophys. Res.*, *99*(A5), 8981–8992.
Rishbeth, H. (1968), Solar eclipses and ionospheric theory, *Space Sci. Rev.*, *8*(4), 543–554.
Rishbeth, H., and O. K. Garriott (1969), *Introduction to Ionospheric Physics*, Academic Press, San Diego, Calif.
Roble, R. G., B. A. Emery, and E. C. Ridley (1986), Ionospheric and thermospheric response over Millstone Hill to the May 30, 1984, Annular Solar Eclipse, *J. Geophys. Res.*, *91*(A2), 1661–1670.
Salah, J. E., W. L. Oliver, J. C. Foster, and J. M. Holt (1986), Observations of the May 30, 1984, Annular Solar Eclipse at Millstone Hill, *J. Geophys. Res.*, *91*(A2), 1651–1660.
Stubbe, P. (1970), The *F*-region during an eclipse—A theoretical study, *J. Geophys. Res.*, *32*, 1109–1116.
Titheridge, J. E. (1997), Model results for the ionospheric *E*-region: Solar and seasonal changes, *Ann. Geophys.*, *15*, 63–78.
Tomás, A. T., H. Lühr, M. Förster, S. Rentz, and M. Rother (2007), Observations of the low-latitude solar eclipse on 8 April 2005 by CHAMP, *J. Geophys. Res.*, *112*, A06303, doi:10.1029/2006JA012168.
Tsai, H. F., and J. Y. Liu (1999), Ionospheric total electron content response to solar eclipses, *J. Geophys. Res.*, *104*(A6), 12,657–12,668.
Tu, J. N., L. Liu, and Z. T. Bao (1997), An low latitude theoretical ionospheric model, *Chin. J. Space Sci. (in Chinese)*, *17*, 212–219.
Walker, G. O., T. Y. Y. Li, Y. W. Wong, T. Kikuchi, and Y. H. Huang (1991), Ionospheric geomagnetic effects of the solar eclipse of 18 March 1988 in East Asia, *J. Atmos. Terr. Phys.*, *53*, 25–37.
Yue, X., W. Wan, L. Liu, H. Le, Y. Chen, and T. Yu (2008), Development of a middle and low latitude theoretical ionospheric model and an observation system data assimilation experiment, *Chin. Sci. Bull.*, *53*(1), 94–101.
Zhang, S. R., X. Y. Huang, Y. Z. Su, and S. M. Radicella (1993), A physical model for one-dimension and time-dependent ionosphere. part I: Description of the model, *Ann. Geofis.*, *36*, 105–110.

H. Le, L. Liu, W. Wan, and X. Yue, Beijing National Observatory of Space Environment, Institute of Geology and Geophysics, Chinese Academy of Sciences, No. 19 Bei Tu Cheng Xi Lu Chaoyang District, Beijing 100029, China. (liul@mail.iggcas.ac.cn)